The Mars 2020 Entry, Descent, and Landing Communications Brownout and Blackout at Ultra-High Frequency

David D. Morabito,* Ewa Papajak,† Trevor Hedges,† David Saunders,† Peter Ilott,‡ Curtis Jin,§ Paul Fieseler,¶ Michael Kobayashi,§ and Mazen Shihabi§

ABSTRACT. — This article discusses the analysis of the ultra-high frequency (UHF) communications blackout and brownout experienced by the Mars 2020 entry vehicle during the period around peak heating of its entry, descent, and landing (EDL) phase into the Martian atmosphere on February 18, 2021. The UHF relay links from Mars 2020 to the Mars Reconnaissance Orbiter and MAVEN orbiter suffered a period of ~60 s of degradation, consisting of a combination of brownout (signal fades) and blackout (complete loss of signal) that coincided with the predicted period of signal degradation from preflight analyses. This article discusses both predictions and measurements of signal degradation that occurred during the peak heating phase of the Mars 2020 EDL. It was found that the model attenuation agreed with measured attenuation, within the factor-of-ten uncertainty of electrons output from the computational fluid dynamics (CFD) tools used in the analysis for most of the signal-degradation period. For cases where there were higher discrepancies between measured and modeled signal attenuation, we have flagged several items for further study, some of which involve various refinements to the CFD tools identified to improve signal-attenuation modeling.

I. Introduction

NASA's Mars 2020 mission arrived at Mars on February 18, 2021, and deployed the Perseverance rover to seek out signs of ancient life and collect rock and regolith samples intended for potential return to Earth. In this study, we report on the signal degradation at ultra-high frequency (UHF, 401 MHz) due to charged particles generated about the

* Communications Architectures and Research Section.

† AMA Inc. at NASA Ames Research Center.

‡ Communications, Tracking, and Radar Section.

§ Flight Communications Systems Section.

¶ Mission Systems Engineering Section.

A portion of the research described in this publication was carried out by the Jet Propulsion Laboratory, California Institute of Technology, under a contract with the National Aeronautics and Space Administration (80NM0018D0004). NASA Ames work was done in the Aerothermodynamics Branch of NASA Ames Research Center and funded by the NASA Space Technology Mission Directorate Entry Systems and Modeling project under a contract NNA15BB15C to AMA, Inc.

spacecraft during the peak heating phase encountered during its entry through the Martian atmosphere. The signals emitted by the Mars 2020 vehicle were received by the Mars Reconnaissance Orbiter (MRO) and Mars Atmospheric and Volatile EvolutioN (MAVEN) orbiter during its entry, descent, and landing (EDL) into the Martian atmosphere. We compare the observed attenuation window with the results predicted by computer simulation.

Several similar analyses were performed for other missions dealing with Mars entries. A description of the general approach and background is provided in [1]. Missions involving signal-degradation analysis during EDL include Mars Phoenix at UHF [2], Mars Science Laboratory (MSL) at UHF [3], and Mars Pathfinder at X-band (8.4 GHz) [1]. A preflight study for the Mars Exploration Rover (MER) vehicles, Opportunity and Spirit, predicted no signal outage due to plasma at the received X-band frequency at the 5.5 km/s entry velocity [1], and indeed no outage due to plasma was observed. The 30-s signal-degradation period was observed for Mars Pathfinder at X-band at its 7.5 km/s entry velocity, and subsequent analysis concluded that most of the outage period was due to charged particle degradation [1]. The European Mars Schiaparelli mission observed a blackout of about 57 s duration during its entry into the Mars atmosphere on October 19, 2016 [4]. Although this period of signal degradation aligned well with their predicted period, their prediction window ended earlier by 10–15 s [5]. This case is similar to what was observed for Mars InSight [6]. Stindt et al. [5] cited several possible reasons for this.

The analysis of the UHF communications blackout and brownout experienced by the more recent Mars InSight spacecraft during entry into the Martian atmosphere on November 26, 2018, is described in detail by Morabito et al. [6]. The UHF relay links from InSight to several receive assets suffered ~52 s of degradation consisting of a combination of brownout (signal fades) and blackout (complete loss of signal). These assets included MRO and the Mars Cube One A (MarCO-A) and MarCO-B CubeSats. The observations agreed with existing models of signal degradation within presently assumed uncertainties given the vehicle's best reconstructed entry trajectory. There were also direct-to-Earth links with near total blackout due to weaker received signal strengths [6,7].

High electron number density along the communication line between transmitter and receiver is likely the dominant contributor to signal degradation. As such, communication attenuation is often calculated as a function of electron number density along line of sight, which can be predicted by computational fluid dynamics (CFD). The amount of ionization for a given size and shape of the entry vehicle is primarily dependent upon atmospheric relative velocity and atmospheric mass density and composition. In the past, the predicted electron number densities were estimated using crude parametric models [1] and the best available trajectory information. The "predicted" outage period occurs when the number density signature as a function of time exceeds the threshold electron number density for the link frequency of interest. These periods identified early in mission development have been used in the building of sequences by mission operations teams. During postflight reconstruction, it has been found that the observed signal degradation aligns well with the predicted outage periods.

For the more rigorous postflight reconstruction analysis, we make use of line-of-sight (LOS) data sets of electron number densities output from CFD tools such as NASA Ames Research Center's Data Parallel Line Relaxation (DPLR) [8] and NASA Langley Research Center's Langley Aerothermodynamic Upwind Relaxation Algorithm (LAURA) [9] real gas flow solvers and ancillary utilities. The results obtained from these CFD tools were based on the reaction rates of Park [10] and will be referred to as the baseline model. The baseline model was used by NASA Langley's LAURA for Phoenix and MSL, and by NASA Ames's DPLR tool for InSight and Mars 2020 [11–12].

An LOS is constructed within a flow solution volume grid according to a body point location on the entry vehicle and a cone and clock angle that direct the LOS towards the intended receiving asset. For this construction, the cone angle is with respect to the vehicle body centerline axis pointing away from the heatshield, which points roughly downstream. The clock angle is the angle (between 0° and 360°) from the body-fixed axis perpendicular to the body centerline and the point of the receive asset projected onto the plane in which the ring antenna lies. Here, the right-handed coordinate system is centered on the body with vehicle's axial reference vector pointing downstream. Deriving these angles from those contained in the telemetry data is beyond the scope of this paper (and nontrivial). Each LOS between a body point and an intersection with the outer grid boundary is discretized with a CFD-like point distribution, then flow field data including electron number density (and possibly pressure and temperature) are interpolated on to the discretization points.

Estimates of measured signal attenuation during the degradation period at chosen time stamps were derived from the difference between signal strength measurements from flight data and the model signal strengths from link analysis [1]. Estimates of modeled signal attenuation come from integrating the electron number density profiles along the signal path traversing the plasma as a function of distance from the vehicle surface towards the relay assets [2].

The integrated electron number density profile along the signal path was multiplied by a factor γ in order to match the model attenuation with the measured attenuation at each time stamp. When these γ factors are near unity, this implies agreement between model and measurement. However, systematic trends were observed as γ increased with time along the trajectory, reaching values of ~3 (and higher) near the end of the degradation period but still within the estimated factor-of-ten uncertainty of electron number density. Previous studies [2,3,6] indicated that CFD tools such as DPLR and LAURA were underestimating electrons. We critically examined CFD models and their inputs to identify any potential refinements due to chemistry, such as ionization and recombination rates, electron-heavy particle collisions, ablation, and radiative heating. The results based on refinements to the baseline model that had been identified to improve signal-attenuation modeling will be the subject of future study.

In this article, we discuss the data sources and tools used in the Mars 2020 analysis (Section II). Next, we discuss the signal-attenuation analysis for both receive assets, MRO and MAVEN (Section III). Then we discuss the Mars 2020 results in the context of those of

previous Mars entry cases and cite possible contributors for the attenuation discrepancies (Section IV). We end with some concluding remarks (Section V).

II. Data Sources and Tools

Trajectory information and other pertinent parameters used in this study include reference time, atmospheric-relative velocity, distance to the center of the planet, atmospheric density, atmospheric pressure, atmospheric temperature, pitch, yaw and roll angles, and sideslip angles. Thus, we made use of the best estimate of the reconstructed trajectory in the J2000 frame. For this study, the two most important quantities extracted with regards to characterizing any blackout or brownout periods were the atmospheric relative velocity and the atmospheric mass density. Figure 1 displays these two quantities for the Mars 2020 entry shortly after traversing the atmospheric interface, defined as the time when the spacecraft is located at a distance of 3,522.2 km from the center of the planet (time = 0 s), which occurred on February 18, 2021, 20:36:48 SCET. The entry velocity at t = 0 s was 5.34 km/s.

As a first-order approximation, the electron number density was roughly estimated using parametric equations, which are functions of atmospheric relative velocity and free-stream atmospheric mass density [1]. The resulting signature of peak electron number density for the stagnation point on the front of the heat shield is shown by the green curve in Figure 2. The results for the wake region electron number density (looking out in the aft direction from the spacecraft) are shown by the orange curve. An estimate of electron number density looking out from the shoulder of the spacecraft (cone angle ~90°) is shown by the intermediate dashed black curve. For reference, the critical electron number density for which signal degradation is expected at the UHF link frequency of 401 MHz is shown by the solid red line at ~2×10^9 cm^{-3}. The wake region curve was found to exceed the critical threshold between 40 s and 90 s past entry, and the shoulder curve exceeds the critical threshold around 30–100 s past entry. We consider the shoulder and wake curves pertinent because communication antennas are located in the rear of the vehicle. The actual received signal levels to the receiving assets do show degradation during these periods from about 50 s to 100 s past entry, as displayed by the purple data

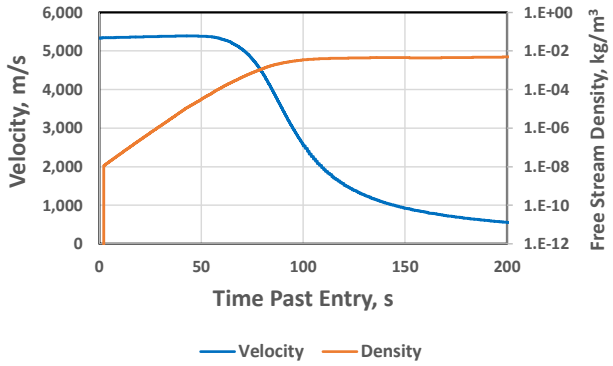

Figure 1. Mars 2020 atmospheric relative velocity and free-stream atmospheric density as a function of time past entry.

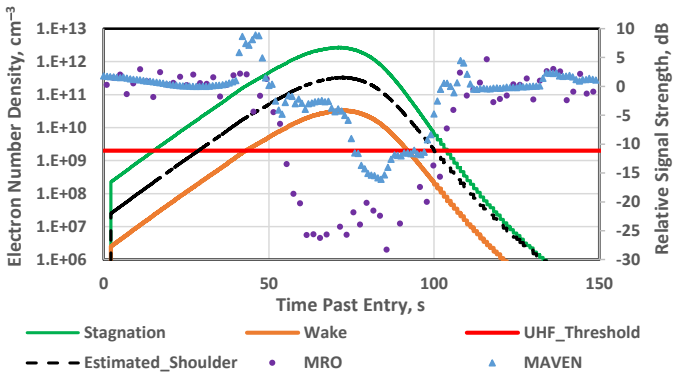

Figure 2. Peak electron number density signatures at stagnation (green), wake (orange), and estimated shoulder mean (dashed black) along with threshold electron number density (red) (left vertical axis). Also shown are the attenuation values estimated from the received signal levels for MRO (purple circles) and MAVEN (light blue triangles) (right vertical axis).

points for MRO and the light blue data points for MAVEN in Figure 2. This period roughly spanned from 20:37:23 to 20:38:25 Spacecraft Event Time (SCET). The period of signal degradation is well correlated with the predicted outage period, when the electron number density curves lie above the threshold limit in Figure 2.

The use of parametric curves in estimating electron number density in Figure 2 is not intended to be the most accurate but does provide a reasonable estimate of the signal-degradation period for which blackout and brownout would occur. These curves based on best available trajectories assist mission planners in generating sequences during EDL. For more accurate estimates, we make use of CFD tools, such as DPLR maintained by NASA Ames. The DPLR package consists of multiple tools used for performing CFD calculations of supersonic and hypersonic flows in chemical and thermal nonequilibrium. DPLR was the primary tool used by NASA Ames in the performance analysis of the thermal protection system of the Mars 2020 entry vehicle. For this study, the existing DPLR flow solutions were reconverged to include the electron number density species in the computed flow fields. Multiple cases about the signal-degradation period involving the Mars 2020-to-MRO and Mars 2020-to-MAVEN signal links were reanalyzed in this manner.

Contour plots of electron number density about the Mars 2020 entry vehicle at various time stamps past entry around the period of peak heating were important in analyzing the signal loss. Figure 3 displays examples of such contour plots. Relevant levels of electron number density were dependent on the direction to the receiving asset at different times during entry. Higher electron densities will be encountered for signal links that transit regions along the shoulder of the vehicle (large cone angles) while lower electron densities will be encountered for signal links along rays through the wake region of the flow (small cone angles) at a given time instant. Note that the plasma on the heat-shield side of the vehicle is greatly compressed (a width of a few cm), while in the wake, the plasma density drops significantly as the flow expands outwards and the positive and negative species recombine over longer distances (a length of up to 30 m).

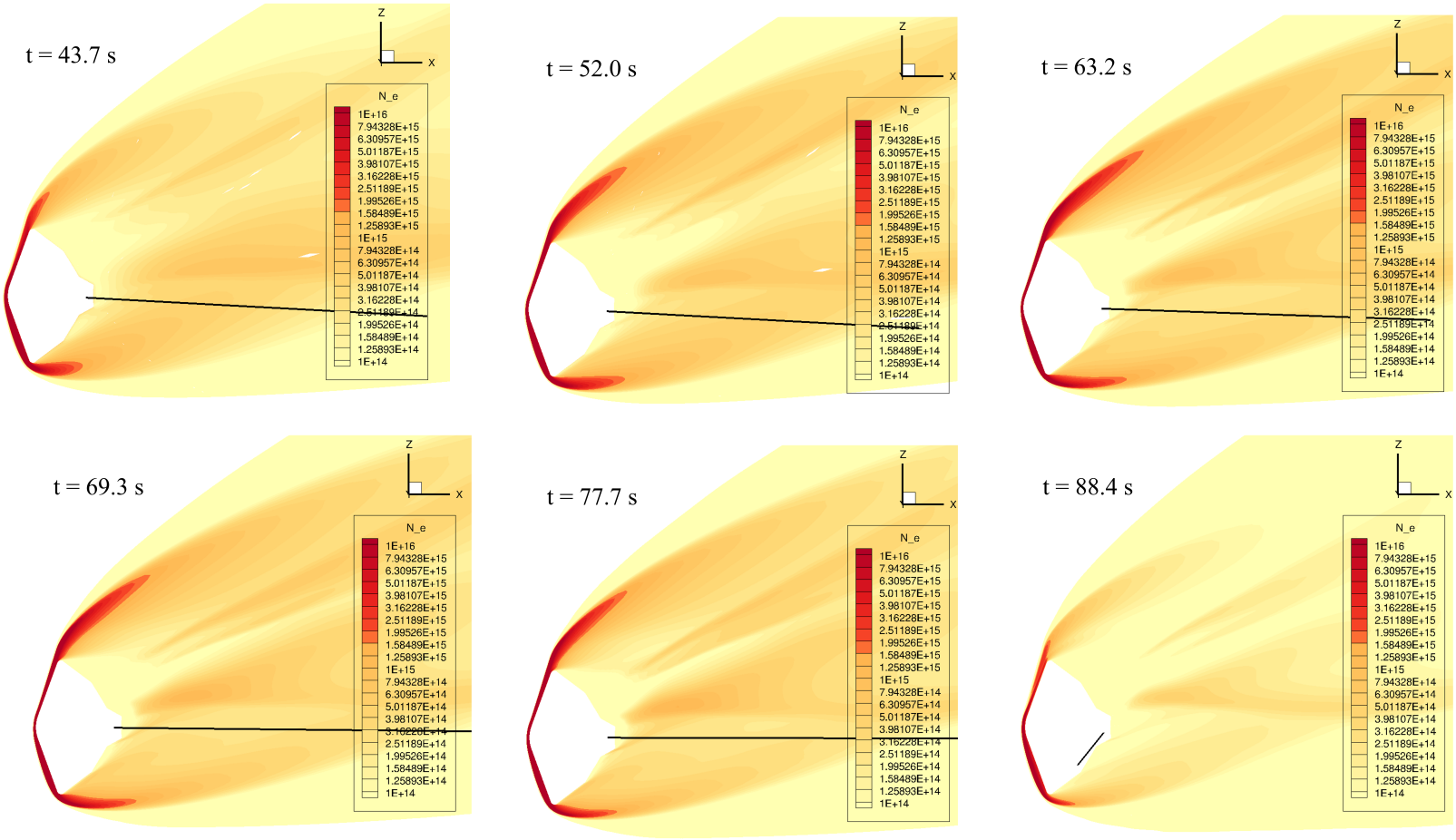

Figure 3. Examples of electron number density contour plots about the Mars 2020 entry vehicle at selected time instances past entry. The range of the electron number densities on the color bar spans from 10^{14} m^{-3} (lightest yellow) to 10^{16} m^{-3} (darkest red). The inserted black lines represent signal paths traversing the plasma in the aft direction from the vehicle.

An example of electron number density as a function of distance from the vehicle along the signal LOS is shown in Figure 4. These are used to produce estimates of signal attenuations at the specific time stamps. The resulting estimates of model signal attenuation are then compared against measured signal attenuation (see Figure 2) during the plasma-degradation period.

The clock and cone angles are shown for Mars 2020 to MRO (Figure 5a) and for Mars 2020 to MAVEN (Figure 5b). We model the signal launch point from the entry vehicle as a point that lies closest to the receive asset lying midway on the wraparound patch UHF (PUHF) antenna ring structure shown in Figure 6.

Within the latter portion of the signal-degradation period (see Figure 2), there were large excursions in the clock and cone angle signatures due to a banking turn that affected the received signal levels. These were used along with the PUHF antenna pattern to estimate predicted signal levels that included all known contributors (e.g., trajectory variations),

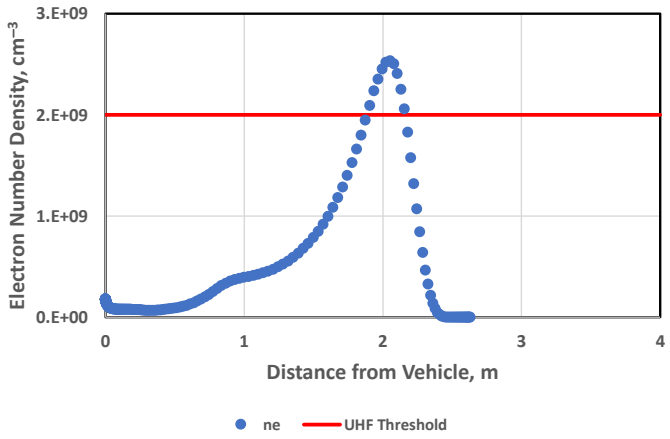

Figure 4. Example of an electron number density profile along the LOS from Mars 2020 to MRO at 52 s past entry. This profile was obtained from DPLR and multiplied by the γ factor obtained to match measured attenuation with model attenuation.

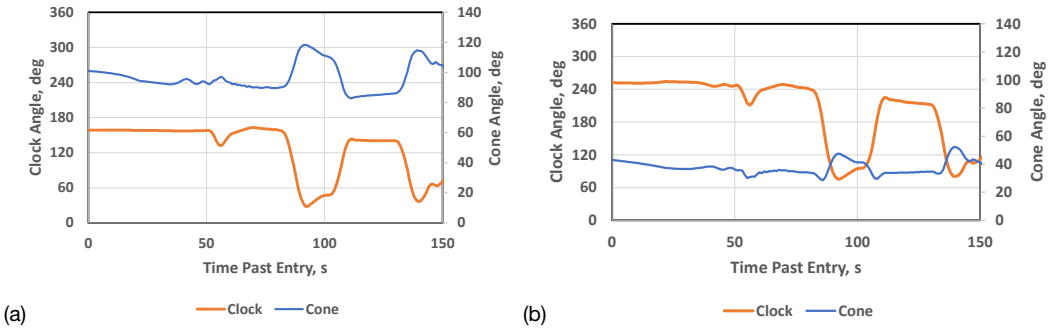

Figure 5. Clock (orange) and cone (blue) angles for a) Mars 2020 to MRO, and b) and Mars 2020 to MAVEN.

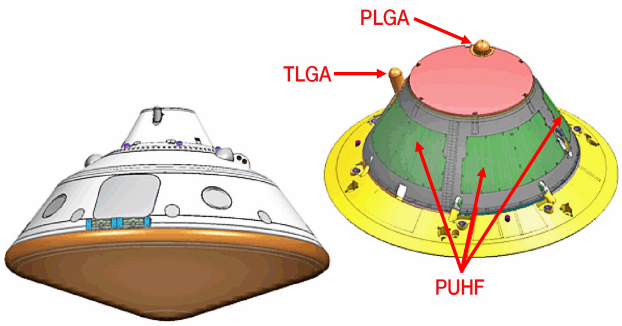

Figure 6. Depiction of the entry vehicle (left) along with a blowup of the aft area (right) showing various antennas, including the wraparound patch antenna (PUHF) used during entry. Credit: Mars 2020 Project. Image taken from [13], Descanso article for MSL-Telecom (nasa.gov). Although this figure pertains to MSL, it is shown for illustrative purposes as Mars 2020 is virtually identical.

but excluded those due to charged particles. By differencing the measured signal strengths with the predicted signal strengths, the measured attenuation levels due to plasma were thus determined. These analyses will be presented in the next section.

III. Analysis

In this section, we discuss the specifics of the Mars 2020-to-MRO signal link (Section III.A) and the Mars 2020-to-MAVEN signal link (Section III.B). Both MRO and MAVEN signal strengths from Mars 2020 were obtained from Automatic Gain Control (AGC) data recorded onboard from their radios that were relayed back to Earth via telemetry.

A. Mars 2020-to-MRO Link

The measured received signal strength data (blue points) and the preflight predicted signal strength (orange points) during the first 150 s past atmospheric entry were examined, as shown in Figure 7a. Also shown in Figure 7b are the clock (dashed orange line) and cone (blue lines) angles towards MRO as seen from the vantage point of the Mars 2020 vehicle. The predicted signal strengths in Figure 7a model all known effects on signal except for the plasma signal degradation.

Referring to Figure 7a, the observed signal-degradation period due to plasma spans from ~48 s to ~110 s past entry. Just outside of the signal-degradation period, the relative signal strength appears fairly stable running near –110 dBm. The received signal at MRO shows a systematic decrease from ~48 s to ~55 s past entry, where it then hits the "noise floor" near –138 dBm at 60 s. There is a short period of smooth signal increase and decrease around 76 s. The signal then emerges from the noise floor from about ~90 s to ~110 s past entry. There are two significant excursions of clock and cone angles (Figure 7b) in the direction of MRO as seen from the Mars 2020 vehicle. During the periods of the large clock/cone excursions shown in the red box between 128 s and 150 s outside of the degradation period, there is a small amount of signal strength variation, ~1–2 dB, consistent with the predictions. During the clock/cone excursions, shown in the green box between 80 s and 110 s within the degradation period, there is significant variation in signal strength from 90 s to 100 s, as the signal is coming out of blackout. Because the two clock/cone signatures

are similar, the variation in signal strength due to the Mars 2020 PUHF pattern variation is assumed to be small. The predictions in Figure 7a show an ~2 dB decrease during this event. In Figure 8, we used the decibel difference between the dashed orange prediction curve model and blue data point measurements (Figure 7a) to obtain measured attenuation to compare with model attenuation from the CFD analysis. A similar approach was employed for the Mars 2020-to-MAVEN link (Section III.B).

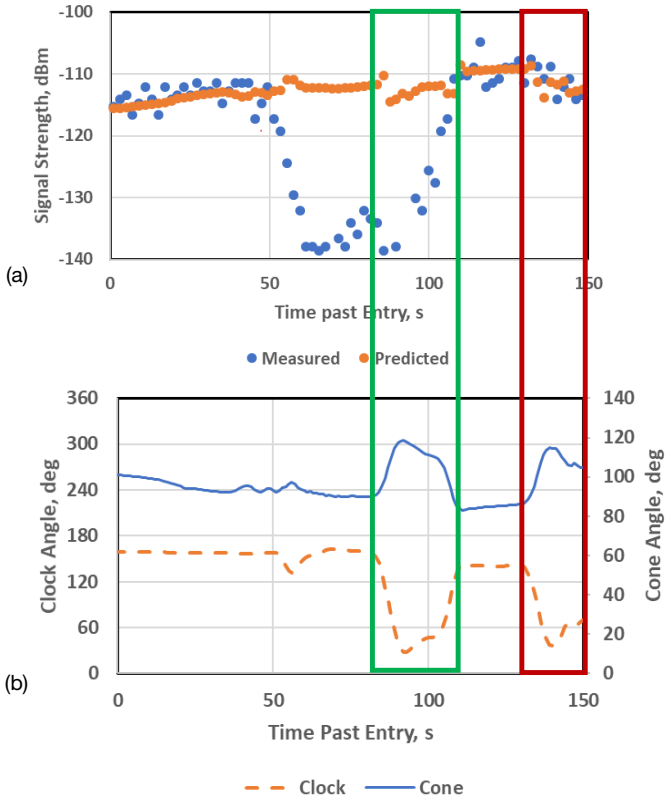

Figure 7. a) Mars 2020-to-MRO received signal levels (blue circles) and predicted signal levels (orange circles). b) clock and cone angles. See text for discussion on the clock/cone excursions within the green and red rectangles.

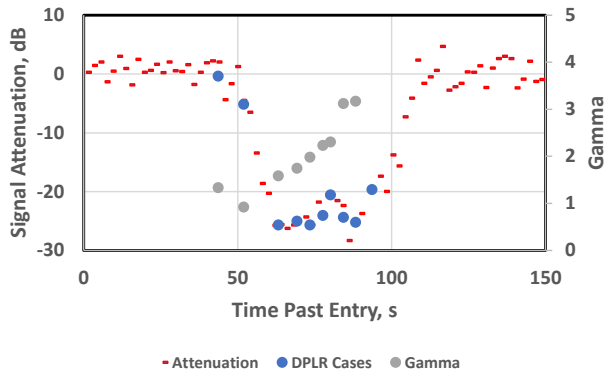

Figure 8. MRO estimated signal attenuation from signal strength measurements and preflight predictions (red dashes), attenuation value at DPLR time stamps of interest (blue circles), and γ values from CFD analysis (gray circles).

The predicted excursions being somewhat small does not seem to cause much of an effect on the received measured signal (maybe a dB or two) inside the red rectangle in Figure 7, unlike the MAVEN excursion, which matched well with the measurements with 3– 4 dB signature (Section III.B). We thus assume the predicted signal strengths have uncertainties of at least ~2 dB.

The attenuation estimates for the Mars 2020-to-MRO link were calculated by differencing the measured relative signal strengths (blue circles in Figure 7a) with the estimated signal strengths (orange dots in Figure 7a), and are shown in Figure 8 as red dashes, where we assume zero attenuation outside of the degradation period. The blue dots in Figure 8 on the attenuation curve denote time stamps in which DPLR CFD analysis was performed, producing electron number density profiles along the specific clock and cone angles at that time stamp. The modeling of attenuation was performed using an integration of the electron number density along the signal path through the plasma as discussed in [2]. The electron number densities in the model were adjusted by a multiplicative parameter, γ, so as to match the measured attenuation with model attenuation. The resulting γ values are shown in Figure 8 as gray circles (right vertical axis label).

The signal decrease between 48–55 s in Figure 8 appears consistent with the attenuation model ($\gamma \sim 1$). The periods prior to "noise floor" in Figure 8 (~–28 dB) and during the small peak at 75 s produce attenuations that are consistent with the measurements ($\gamma \sim 1$–2), well within the uncertainty of DPLR estimation of electron number density ($|\gamma| < 10$). However, the attenuations for the period during signal increase (from 90 s to 100 s) cannot be explained by the electron number density model, which requires adjustment factors that exceed the expected order-of-magnitude uncertainty of the electron number density (γ not shown for these points in Figure 8). The Electra radio on MRO would not show such a signal increase signature over the 10 s from 90 s to 100 s past entry as signal acquisition, which would be nearly instantaneous in the absence of electrons. The γ values estimated during the period around the noise floor from 64 s to 90 s are reasonable at ~1–2, where we assume the received signal level lies at or just below the detection threshold. It should be borne in mind that due to the banking turn and high cone angles (>90°), the predicted signal levels are not expected to be accurate, so that the attenuation accuracy could be off by 2 or more dB as previously alluded to. Whether this is a valid assumption or not, the resulting γ values prior to this point are reasonable.

B. Mars 2020-to-MAVEN Link

In order to access measured signal attenuation, the received signal strength data were examined, as shown in the example of the MAVEN received AGC signal strength (blue points) and predicted signal strengths (orange points) in Figure 9a during the first 150 s past atmospheric entry. Also shown are the clock and cone angles towards MAVEN as seen from the vantage point of the Mars 2020 vehicle (Figure 9b). The green and red boxes denote periods where there were large excursions in the clock and cone angles due to events such as banking turns. One can see that the predictions show excursions as large as ~4 dB during these periods.

The measured AGC signal levels (blue) were differenced from the signal levels expected assuming no plasma effects (orange) in Figure 9a to produce the attenuation values shown

in Figure 10a. The large signal excursion (~5–10 dB) that lies above 0 dB just before the signal degradation period (at ~40 s past entry) in Figure 10a is likely related to spacecraft mode changes. The signal excursion just after the signal-degradation period of ~5 dB at ~110 s past entry is not yet understood. Figure 10b shows the resulting γ values, which were derived after matching model attenuation with the measured attenuation.

With regards to Figure 10b, the resulting γ values across all DPLR points show a smooth systematic trend even through the expected "noise floor." This suggests that the signal attenuation was lying close to the threshold. The systematic increase near the end of the degradation period from about 70 s to 94 s past entry is suggestive of trends seen in other

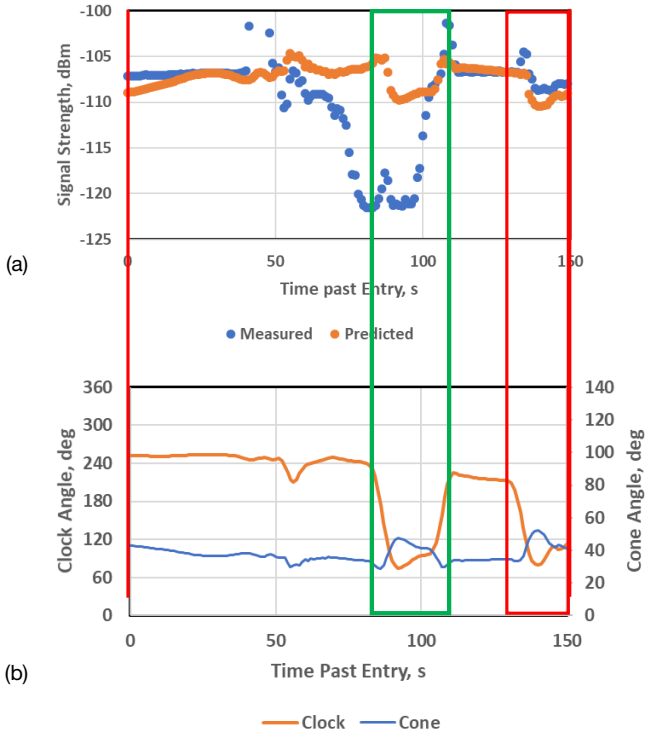

Figure 9. a) Received signal levels at MAVEN (blue) and predicted signal levels (orange); b) Mars 2020-to-MAVEN clock and cone angles.

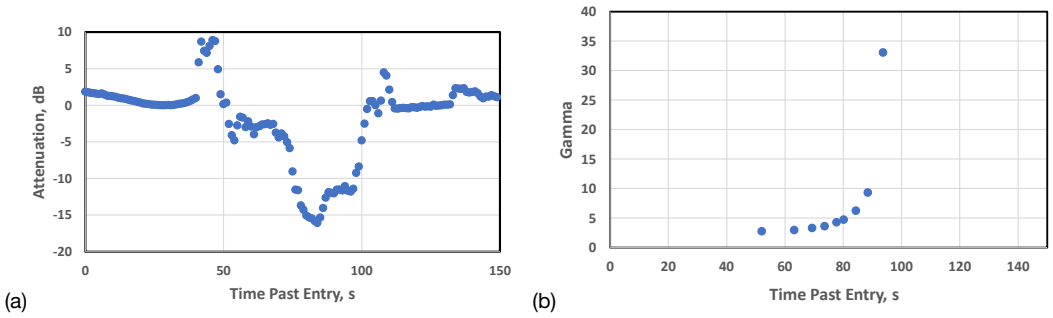

Figure 10. Mars 2020-to-MAVEN signal link a) attenuation values and b) γ values.

data sets (e.g., InSight [6]). At the start of the degradation period, the resulting γ values cluster around ~3, which is higher than the expected values of near unity seen for other data sets at this time. However, these values are within the assumed factor-of-ten uncertainty of electron number density output from DPLR, but it must be kept in mind that the MAVEN link direction was at low cone angles looking out in the wake region, where there may be higher uncertainties associated with the sparser, more tenuous plasma densities over the longer few-meter span. This is in contrast to the shorter plasma spreads closer to the vehicle, such as with the MRO link looking more in the shoulder directions (higher cone angles).

IV. Discussion

As seen in Figures 8 and 10b, there is an apparent trend in γ increasing during the signal-degradation period as the atmosphere becomes denser. Similar trends have been observed in the analyses of other Mars entries. Figure 11 displays γ factors for various Mars entry signal links as functions of time past entry, including selected cases from this study added to the previously published plot of Figure 15b in Reference [6]. The values in Figure 11 include those for this recent study: the Mars 2020-to-MRO link (black diamonds) and the Mars 2020-to-MAVEN link (black squares). All of these values lie between 0.1 and 10 and are thus within the factor-of-ten uncertainty of the electron species output by the LAURA and DPLR tools. (We assume that the LAURA solutions [9] should have a similar uncertainty in electron number density calculations compared to DPLR.) The Mars 2020 γ values (up to 88 s past entry) all lie within the factor-of-ten uncertainty of electron number density, showing similar trends (increasing as atmospheric density increases) to those estimated from other missions.

The Mars 2020-to-MRO link γ values average ~1.7 at an average cone angle of 91°, while those of the Mars 2020-to-MAVEN link average ~3.6 over an average cone angle of 35° (see Figure 12). There is a rough but apparent trend with cone angle, where γ values of 1–2

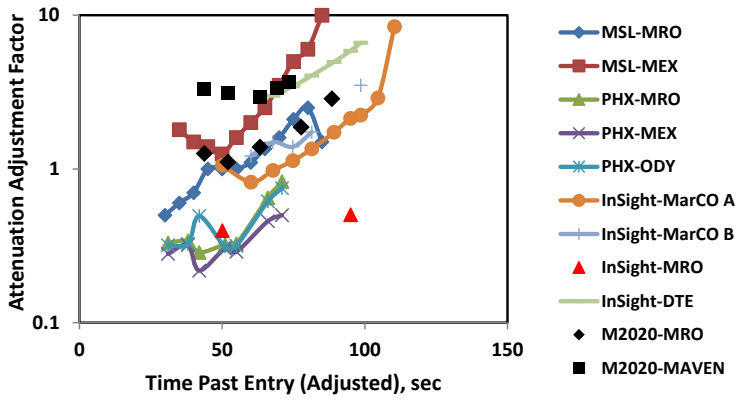

Figure 11. γ factors for various Mars entry signal links as functions of time past entry from [6] with Mars 2020 values added (black symbols). See text.

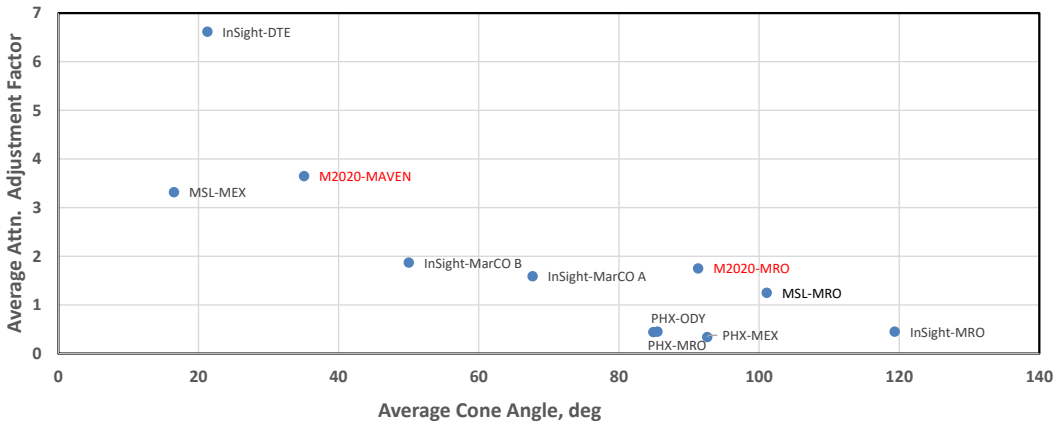

Figure 12. Average γ versus average cone angle. Recent Mars 2020 labels shown in red.

imply more accurate estimation of electrons by the CFD tools at higher cone angles near or approaching the vehicle shoulders (>50°), whereas higher γ values are experienced at lower cone angles (<40°) where the signal links are looking out into the aft direction of the vehicles through longer, more sparse and tenuous plasma paths. It is believed that the estimation of electron number density should be better modeled along the shoulder direction, where it is closer to the flows spewing off the heat shield and the span is shorter (on an order of centimeters), versus looking more in the aft direction, where the flow is of longer span (on an order of meters), more tenuous and sparser, and thus may have higher uncertainties.

The deviation of γ factors from unity shown in Figure 11 was investigated in an internal JPL study for several cases of spacecraft and EDL phases during the signal-degradation period. For the most part, the γ values lay within the factor-of-ten uncertainty of the electron number density output by the CFD tools. During the study, the concentrations of chemical species (primarily ions and electrons) were studied for both stagnation line and aft regions in order to identify species that may contribute to any discrepancy between model and measurement attenuations. The case of the InSight-to-MarCO-A link was the main focus of the study because it involved more data points during signal lock and the γ signature showed a reasonably smooth increasing systematic trend (orange circles in Figure 11).

These results were examined more closely by inspecting the number densities of the various positive ion species. It was found that the raw electron number density peaks near 70 s past entry and that the dominant positive ion at that time is NO^+, which peaks near 75 s past entry. All of the other positive ions lie below these levels by a factor of 2.5 and more compared to the number density of NO^+. Because peak concentrations of electrons correlate well with peak concentration of NO^+, formation of NO^+ can be postulated to be the main mechanism of ionization of plasma during Mars entry. This reaction involves associative ionization (AI) of atomic oxygen O and atomic nitrogen N into NO^+ and produces free electrons: $N + O <-> NO^+ + e^-$. If N + O AI is the main source of electrons, the uncertainty in the N + O AI rate coefficient could also be responsible for the large γ factors at the end of the plasma-communication-degradation period. Another possibility is that uncertainties in electron-impact ionizations or subsequent recombination reactions also contribute to large γ factors in the later times.

The chemistry model in DPLR calculations for the InSight entry involves 17 species and 35 reactions [10]. The AI rate used in DPLR made use of the rate coefficients from [9,10]. This reaction rate was based on Earth-atmosphere-chemistry work done in the 1960s [15,16]. It was also found that the electron concentration could be underestimated by a factor of ~3.6 [17,18].

Papajak et al. [19] calculated this rate using modern quantum chemistry and found that the older rate is significantly low. Future work will involve exploring the impact of this and other reactions on the electron density along LOS and their possible impact on γ factors at times near the end of the signal-degradation period. A forthcoming paper will include discussion of these results in detail.

Various other possible contributors to the uncertainty of electron numbers include ablation, radiation, and the complexity of the attenuation model as it was applied.

DPLR does not have built-in materials response models, and thus our analysis did not account for ablation of the heat-shield material. Up to now, all of our analyses have neglected ablation as it has been assumed negligible. Possible future work would involve at least quantifying the contribution due to ablation.

One would expect radiative heating to contribute to overall temperature increase, which in turn would cause higher ionization reaction rates and hence more electrons. Increased radiative flux magnitudes occur when the atmosphere is denser, such as during the end of the plasma signal-degradation period. The majority of Mars entry cases had entry velocities lower than 6 km/s, where radiative heating was deemed insignificant compared to convective heating [14]. For the case of Mars Pathfinder, with an entry velocity ~7 km/s, radiative heating was found to be significant on the aft body compared to convective heating due to species recombination in the wake region. For the InSight analysis, the electron density profiles during transit during the period of denser atmosphere needed to be increased substantially in order to match the attenuation model with attenuation measurements. Thus, radiative heating may be one factor causing more electrons to be produced during the latter stages of the signal-degradation period. Although radiation as a free electron contributor is not expected to be significant, it should be investigated to quantify its contribution. A forthcoming version of DPLR will permit radiation coupling.

Although the plasma produced during entry is effectively inhomogeneous in both electron density and collision frequency, the collision-frequency inhomogeneity merited very little attention in the past [20]. The signal-attenuation model used in our analysis neglects the impact of local pressure and temperature on the frequency of electron-heavy particle collisions. Given that our analysis showed that electron number densities generally were less than $10^{10}/cm^3$ for the attenuation values measured, one could expect negligible difference between the two attenuation models involving collisions and no collisions. However, our analysis suggests that the effect of collisions should be examined more closely. It can be hypothesized that by employing an appropriate collision-inclusive model, one could obtain a better qualitative match to the measured curve and reduce the γ values. This, along with gaining a more detailed insight into uncertainties from individual reactions, will be revisited in future studies.

V. Conclusion

We presented the results of the signal-degradation analysis due to charged particles of the Mars 2020 mission during the period around peak heating during its EDL into the Martian atmosphere on February 18, 2021. The signals emitted by the Mars 2020 vehicle were received by the MRO and MAVEN orbiters. It was found that the model-attenuation predictions agreed with measured attenuation measurements, within the factor-of-ten uncertainty of electrons output from the CFD tools used in the analysis for most of the signal-degradation period. For cases where there were higher discrepancies between measured and modeled signal attenuation, we have identified several items for further study, some of which involve various refinements to the CFD tools identified to improve signal-attenuation modeling.

The results of this work can benefit forthcoming Mars missions involving hypersonic atmospheric entries (e.g., Mars Sample Return), lowering the uncertainties of various CFD real gas chemistry parameters. This would include reducing the uncertainty of predicted electron number density below its putative factor-of-ten values for NASA's present flow solvers, DPLR and LAURA. Such work could also be beneficial for better assessment of heat-shield performance as well as assessing and predicting radio blackout/brownout durations. From a scientific standpoint, the work performed here can result in the improvement and validation of reaction rate formulation applicable to the Martian atmosphere.

Acknowledgments

We would like to thank Dinesh Prabhu of NASA Ames for many helpful discussions on this study as well as valuable suggestions and for providing the additional data sets needed to realize this study. We thank Richard Jaffe of NASA Ames for invaluable comments on the chemistry and kinetics of reactions in ionized plasma. We also thank Frederick Serricchio of JPL for providing the Mars 2020 spacecraft trajectory parameters used in the analysis. Part of the present work was carried out in the NASA Aerothermodynamics Branch of NASA Ames Research Center and funded by the NASA Space Technology Mission Directorate Entry Systems and Modeling project under a contract NNA15BB15C to AMA, Inc. The rest of the research was carried out at the Jet Propulsion Laboratory, California Institute of Technology, under a contract (80NM0018D0004) with the National Aeronautics and Space Administration. We also acknowledge additional funding provided by Roy Gladden of the Mars Exploration Program Office at JPL.

References

[1] D. D. Morabito, "The Spacecraft Communications Blackout Problem Encountered During Passage or Entry of Planetary Atmospheres," *Interplanetary Network Progress Report,* vol. 42-150, Jet Propulsion Laboratory, Pasadena, California, pp. 1–23, August 15, 2002. https://ipnpr.jpl.nasa.gov/progress_report/42-150/150C.pdf

[2] D. D. Morabito, R. Kornfeld, K. Bruvold, L. Craig, and K. Edquist, "The Mars Phoenix Communications Brownout during Entry into the Martian Atmosphere,"

Interplanetary Network Progress Report, vol. 42-179, Jet Propulsion Laboratory, Pasadena, California, pp. 1–20, November 15, 2009. https://ipnpr.jpl.nasa.gov/progress_report/42-179/179A.pdf

[3] D. D. Morabito, B. Schratz, K. Bruvold, P. Ilott, K. Edquist, and A. Dwyer Cianciolo, "The Mars Science Laboratory EDL Communications Brownout and Blackout at UHF," *The Interplanetary Network Progress Report,* vol. 42-197, Jet Propulsion Laboratory, Pasadena, California, May 15, 2014. https://ipnpr.jpl.nasa.gov/progress_report/42-197/197A.pdf

[4] A. Aboudan, G. Colombatti, C. Bettanini, F. Ferri, S. Lewis, B. Van Hove, O. Karatekin, and S. Debei, "ExoMars 2016 Schiaparelli module trajectory and atmospheric profiles reconstruction: analysis of the on-board inertial and radar measurements," *Space Science Reviews*, vol. 214, pp. 1–31, 2018. https://link.springer.com/article/10.1007/s11214-018-0532-3

[5] T. Stindt, J. Merrifield, D. Evans, and L. Ferracina, "Numerical computation of ExoMars Schiaparelli communications blackout compared with flight," *International Conference on Flight Vehicles, Aerothermodynamics and Re-entry Missions and Engineering (FAR).* At Torre Cintola Nature Sea Resort, Monopoli, Italy, September 30–October 3, 2019. https://www.researchgate.net/publication/336587840_Numerical_Computation_of_ExoMars_Schiaparelli_Communications_Blackout_Compared_with_Flight

[6] D. D. Morabito, et al., "InSight communications degradation during peak heating phase of atmospheric entry," *Journal of Spacecraft and Rockets,* vol. 58 (3), May–June 2021.

[7] S. M. Krasner, K. Bruvold, J. A. Call, P. D. Fieseler, A. T. Klesh, M. M. Kobayashi, N. E. Lay, R. S. Lim, D. D. Morabito, K. Oudrhiri, M. Wallace, A. H. Grimes, T. Palagi, D. K. Litton, G. M. Signori, and A. S. McEwen, "Reconstruction of entry, descent, and landing communications for the interior exploration using seismic investigations, geodesy, and heat transport Mars Lander," *Journal of Spacecraft and Rockets,* September 21, 2021. https://doi.org/10.2514/1.A34892

[8] M. W. Wright, T. White, and N. Mangini, "Data parallel line relaxation (DPLR) code user manual Acadia—version 4.01.1," *NASA TM-2009-215388,* October 2009.

[9] P. A. Gnoffo, R. N. Gupta, and J. L. Shinn, "Conservation equations and physical models for hypersonic air flows in thermal and chemical non-equilibrium," *NASA Technical Paper 2867,* National Aeronautics and Space Administration, Hampton, Virginia, 1989.

[10] C. Park, J. T. Howe, R. L. Jaffe, and G. V. Candler, "Review of chemical-kinetic problems of future NASA missions. II - Mars entries," *Journal of Thermophysics and Heat Transfer,* vol. 8 (1), pp. 9–23, January 1994.

[11] A. M. Brandis, C. O. Johnston, B. A. Cruden, D. K. Prabhu, A. A. Wray, Y. Liu, D. W. Schwenke, and D. Bode, "Validation of CO 4th positive radiation for Mars entry," *Journal of Quantitative Spectroscopy and Radiative Transfer*, vol. 121, pp. 91–104, May 2013. https://www.sciencedirect.com/science/article/pii/S0022407313000630

[12] A. Brandis, C. Johnston, M. Panesi, B. Cruden, D. Prabhu, and D. Bose, "Investigation of nonequilibrium radiation for Mars entry." In *51st AIAA Aerospace Sciences Meeting, including the New Horizons Forum and Aerospace Exposition,* Grapevine (Dallas/Ft. Worth Region), Texas, pp. 1055, June 7–10, 2013. http://arc.aiaa.org/doi/pdf/10.2514/6.2013-1055

[13] A. Makovsky, P. Ilott, and J. Taylor, "Mars Science Laboratory Telecommunications System Design*," DESCANSO Design and Performance Summary Series,* Article 14, Jet Propulsion Laboratory, Pasadena, California, November 2009. https://descanso.jpl.nasa.gov/DPSummary/Descanso14_MSL_Telecom.pdf

[14] C. O. Johnston, A. M., Brandis, and K. Sutton, "Shock layer radiation modeling and uncertainty for Mars entry," *43rd AIAA Thermophysics Conference,* New Orleans, Louisiana, June 25–28, 2012.

[15] M. G. Dunn and J. A. Lordi, "Measurement of electron temperature and number density in shock tunnel flows, Part 2: NO^+ + e dissociative recombination rate in air," *AIAA Journal,* vol. 7, pp. 2099–2104, November 1969.

[16] S. C. Lin, "Ionization phenomenon of shock waves in oxygen-nitrogen mixtures," *Research Rept. 33,* Avco-Everett Research Laboratory, Everett, Massachusetts, June 1958.

[17] J. S. Evans and P. W. Huber, "Calculated radio attenuation due to plasma sheath on hypersonic blunt-nosed cone," *NASA Technical Note NASA TN D-2043,* December 1963.

[18] S.-C. Lin and J. D. Teare, "Rate of ionization behind shock waves in air; II. Theoretical Interpretations," *The Physics of Fluids,* vol. 6 (3), pp. 355–375, March 1963.

[19] E. Papajak, W. M. Huo, D. W. Schwenke, and R. L. Jaffe, "Dissociative Recombination (DR) and Associative Ionization (AI) Cross Section Calculations for the NO^+ + e yields N + O (^{2}D+^{3}P, ^{2}P+^{3}P, and ^{2}D+^{1}D) Reaction for Atmospheric Entry Modeling," *The 74th Annual Gaseous Electronics Conference,* 2021. https:/ntrs.nasa.gov/citations/20210017590

[20] Li-Xin Guo and Lin-Jing Guo, "The effect of the inhomogeneous collision frequency on the absorption of electromagnetic waves in a magnetized plasma," *Physics of Plasmas,* vol. 24 (11): 112119, November 2017. https://doi.org/10.1063/1.5012769